# A Preliminary Study to Enhance the Tribological Performance of CoCrMo Alloy by Fibre Laser Remelting for Articular Joint Implant Applications

**Chi-Wai Chan [1,*], Graham C. Smith [2] and Seunghwan Lee [3]**

[1] Bioengineering Research Group, School of Mechanical and Aerospace Engineering, Queen's University Belfast, Belfast BT9 5AH, UK
[2] Department of Natural Sciences, University of Chester, Thornton Science Park, Chester CH2 4NU, UK; graham.smith@chester.ac.uk
[3] Department of Mechanical Engineering, Technical University of Denmark, DK-2800 Kgs. Lyngby, Denmark; seele@mek.dtu.dk
* Correspondence: c.w.chan@qub.ac.uk

Received: 31 January 2018; Accepted: 27 February 2018; Published: date

**Abstract:** CoCrMo alloy has long been used as a pairing femoral head material for articular joint implant applications because of its biocompatibility and reliable tribological performance. However, friction and wear issues are still present for CoCrMo (metal)/CoCrMo (metal) or CoCrMo (metal)/ultrahigh molecular weight polyethylene (UHMWPE) (plastic) pairs in clinical observations. The particulate wear debris generated from the worn surfaces of CoCrMo or UHMWPE can pose a severe threat to human tissues, eventually resulting in the failure of implants and the need for revision surgeries. As a result, a further improvement in tribological properties of this alloy is still needed, and it is of great interest to both the implant manufacturers and clinical surgeons. In this study, the surface of CoCrMo alloy was laser-treated by a fibre laser system in an open-air condition (i.e., no gas chamber required). The CoCrMo surfaces before and after laser remelting were analysed and characterised by a range of mechanical tests (i.e., surface roughness measurement and Vickers micro-hardness test) and microstructural analysis (i.e., XRD phase detection). The tribological properties were assessed by pin-on-disk tribometry and dynamic light scattering (DLS). Our results indicate that the laser-treated surfaces demonstrated a friction-reducing effect for all the tribopairs (i.e., CoCrMo against CoCrMo and CoCrMo against UHHMWPE) and enhanced wear resistance for the CoCrMo/CoCrMo pair. Such beneficial effects are chiefly attributable to the presence of the laser-formed hard coating on the surface. Laser remelting possesses several competitive advantages of being a clean, non-contact, fast, highly accurate and automated process compared to other surface coating methods. The promising results of this study point to the possibility that laser remelting can be a practical and effective surface modification technique to further improve the tribological performance of CoCr-based orthopaedic implants.

**Keywords:** laser remelting; fibre laser; CoCrMo alloy; tribological performance; wear resistance

## 1. Introduction

With the increasing life-expectancy and active lifestyles of the elderly population of modern society, the number of articular joint prosthetic surgeries, e.g., total hip replacement (THR) and total knee replacement (TKR), is ever increasing [1–3]. Unlike other implants, articular joint implants are designed to function under persistent loading and shear stress. For this reason, wear has long been recognized as the principal cause of inflammatory bone loss [4,5]; the particulate wear debris can initiate a cascade of adverse tissue responses including osteolysis (bone resorption), aseptic loosening

and implant failure, often resulting in the need for late revision surgeries. Thus, it is critical to develop and/or employ materials that show highly wear-resistant properties as bearing materials. Presently, one of the most prevalent femoral head materials is CoCrMo alloy, while either CoCrMo or ultrahigh molecular weight polyethylene (UHMWPE) is used as the mating pair [1–3,6,7]. Despite excellent biocompatibility and reliable tribological performance, however, friction and wear issues are still persistent even for CoCrMo/CoCrMo or CoCrMo/UHMWPE pairs [1–3,6,7]. Particularly, the very small-sized wear particles generated from the CoCrMo-on-CoCrMo bearing surfaces have a large surface-to-volume ratio, which could promote the release of Cr and Co ions into the host body [8]. It is thus of interest to determine whether the tribological properties of these bearing materials can be further improved, aiming to minimize the generation of such wear debris from the wearing process.

Attempts to improve the wear resistance of CoCr-based alloys have been made in the literature using different surface modification methods, including plasma surface alloying with N and C [9] or plasma nitriding [10], electron beam surface treatment [11], deposition of hard coatings, namely titanium nitride (TiN) [12–14] and diamond-like carbon (DLC) [15,16], by physical vapour deposition (PVD) or deposition of DLC [17] by chemical vapour deposition (CVD). In this study, we are primarily interested in improving the tribological properties of CoCrMo by means of laser processing.

Existing literature related to the laser processing of CoCrMo alloy can be grouped into two main categories, namely (i) laser cladding of the CoCrMo layer onto other substrates and (ii) laser 3D printing of the CoCrMo solid part. The findings related to laser cladding can be summarised in chronological order as follows: Meacock and Vilar studied the deposition of CoCrMo layer onto 304 stainless steel by laser cladding [18]. Their findings indicated that the laser-induced fine microstructure can increase the hardness of CoCrMo. Chen et al. applied a continuous wave (CW) mode $CO_2$ laser to deposit a CoCrMo cladding layer onto 718H mould steel [19]. Their laser-cladded CoCrMo layer demonstrated an increased hardness (i.e., HV 794) and enhanced wear resistance. Barekat et al. performed a series of studies to investigate different coating characteristics [20,21] and wear behaviour [22] of laser-cladded CoCrMo on $\gamma$-TiAl substrate using a Nd:YAG laser. The findings related to laser 3D printing are as follows: Monroy et al. applied a fibre laser to produce CoCrMo solid parts using the selective laser melting technique (SLM) [23]. The CoCrMo parts created by the SLM process exhibited superior hardness than those produced by conventional manufacturing processes (e.g., casting, electron beam melting and forging). Mantrala et al. created a CoCrMo layer using the laser-engineered net shaping (LENS) technique [24]. They reported that the microstructural features, as well as the hardness and wear properties strongly depended on the laser processing parameters. In their follow-up study [25], they reported that post heat-treatment can improve the wear resistance by increasing the hardness (i.e., HV 512). Sahasrabudhe et al. applied the LENS technique to increase the wear resistance of CoCrMo with the addition of calcium phosphate (CaP) in the laser-printed parts [26].

The abovementioned studies indicate the possibility of increasing the hardness and wear resistance of CoCrMo alloy by laser processing. We have recently demonstrated that laser surface remelting (hereafter, called laser remelting) of metallic materials, for example titanium or titanium-based alloys, leads to a greatly enhanced wear-resistance [27,28]. Meanwhile, corresponding studies on CoCrMo surface are relatively rare.

Laser remelting is an effective approach to modify the surface structure and properties of metallic materials, such as roughness, hardness and corrosion resistance [29,30]. It is commonly employed as a post-process treatment for enhancing the homogeneity in microstructure and reducing the porosity in the surface layer [31–34]. Examples of successful applications to bio-metallic materials include AISI 316L stainless steel [31] and Ti6Al4V [34]. Unlike the more popular technique, namely laser ablation (or laser surface texturing), which is based on the removal of material to create the surface patterns, laser remelting modifies the surface based on the reallocation of material while in its molten state (i.e., no material is removed when the surface is irradiated by a laser beam) [29]. The surface remains below the material vaporisation temperature throughout the laser remelting process, whereas it is above in the case of laser surface texturing [35].

Laser remelting possesses several competitive advantages of being a clean, non-contact, fast, highly accurate and automated process compared to the abovementioned surface modification methods. The majority of them (i.e., plasma nitriding, PVD and electron beam treatment) required a gas or vacuum chamber, which was only specific to the research group that used it, and it greatly increases the cycle time of the treatment process. Our newly-modified laser remelting technique provides an additional benefit of no involvement of a gas chamber. It can be applied directly to the curved implant surfaces in an open-air condition. Further, the surface layer formed by laser remelting is metallurgically bonded with the substrate, and thus, it has no concern of coating delamination (i.e., the main problem for the hard coatings deposited by the PVD method).

To the best of the authors' knowledge, only a very limited amount of research work has been devoted to investigate the enhancement of wear resistance of CoCrMo alloy by laser remelting in the context of articular joint implant applications. This became the motivation to conduct this study.

## 2. Materials and Methodologies

### *2.1. Materials*

The material used in the laser remelting experiment was CoCrMo alloy, which was purchased from Zapp Precision Metals GmbH (Schwerte, Germany). The samples were fabricated in the form of cylindrical pins with a flat end (the diameter was ca. 7 mm in the stem, yet reduced to ca. 3.4 mm at the end) and discs (30 mm in diameter and 5 mm in thickness), respectively. The sample surface was ground sequentially with a series of sandpapers from 120 to 400 grit following the standard metallography procedure. The purpose of grinding was to (1) remove the pre-existing oxides and (2) ensure surface homogeneity/consistency in roughness. After grinding the surface, the samples were cleaned in an ultrasonic ethanol bath for 10 min, rinsed in distilled water for another 10 min and then dried completely in a cold air stream. Ultrahigh molecular weight polyethylene (UHMWPE) was purchased from Orthoplastics Ltd. (Crosslinked, GUR 1020 Compression moulded, Lancashire, UK) and was fabricated to a pin with a flat end (ca. 7.4 mm in diameter) and a disc (30 mm in diameter and 5 mm in thickness). From these two materials, three tribopairs, namely (a) CoCrMo pin-on-CoCrMo disc, (b) UHMWPE pin-on-CoCrMo disc and (c) CoCrMo pin-on-UHMWPE disc, were prepared. (b) and (c) are composed of the same pair of materials, but the configuration of the slider/disc was opposite. Moreover, the diameters of the UHMWPE pin and CoCrMo pin were somewhat different. Foetal bovine serum (FBS) was purchased from Sigma (Brøndby, Denmark).

### *2.2. Laser Remelting Experiment*

The laser remelting experiment was carried out using an automated continuous wave (CW) 200 W fibre laser system (MLS-4030), which was integrated by Micro Lasersystems BV (Driel, The Netherlands). The fibre laser was manufactured by SPI Lasers UK Ltd. (Southampton, UK), and the wavelength of the laser was 1064 nm. The sample surface was laser-treated using the following optimised processing parameters: laser power 40 W, scanning speed 25 mm/s (i.e., meandered scan with lateral movement of 100 μm in the horizontal direction), stand-off distance 1.5 mm (i.e., laser spot size was measured as approximately 100 μm) and shielding with the high purity $N_2$ at 5 bar. The optimised set of processing parameters was determined in a preliminary experiment. The objective of this preliminary experiment was to create a defect-free surface, i.e., no surface discolouration and cracks. The $N_2$ gas was coaxially delivered with the laser beam to the surface via a standard laser nozzle. The laser-treated area was 18 × 18 mm on the disc sample and completely covered the flat surface at the end of the pin sample (ca. 3.4 mm in diameter). The laser-treated area was fully covered with laser tracks, and the overlapping ratio between the tracks was about 50% in track width. The detail of the laser remelting setup was given in the authors' previous study [36]. The CoCrMo samples after laser remelting are denoted as CoCrMo*.

*2.3. Surface Morphology and Phase Structure Analysis*

The surface before and after laser remelting was imaged using an optical microscope. The surface phase structure was characterized by XRD using a Bruker D8 Advance diffractometer in Bragg–Brentano ($\theta/2\theta$) geometry with Cu $K_\alpha$ radiation, a fixed divergence slit and a Ni $K_b$ suppression filter. Data were scanned from 32° to 82° in $2\theta$ using 0.005° steps. The penetration depth of X-rays into the sample during the XRD measurements was estimated using the method of Cullity [37], with a weighted mass absorption coefficient for Cu K$\alpha$ X-rays taken from NIST standard reference data for a CoCrMo composition corresponding to the average for ASTM F-75 medical-grade material [38]. Results showed an information depth varying from approximately 0.8 μm at $2\theta$ = 32° up to approximately 1.9 μm at $2\theta$ = 82°.

The measured peak positions in the XRD analysis are shown in the Table 1 below. Peak assignments follow those of Guo et al. [39]. Note that the $\alpha$ and $\varepsilon$ phase peaks at approximately 41° and 75° were not separately resolved in these measurements.

**Table 1.** Measured peak positions in XRD for CoCrMo before and after laser remelting.

| Peak Assignment | Measured Peak Position | |
|---|---|---|
| | Before Laser Remelting | After Laser Remelting |
| $\alpha$ (100)/$\varepsilon$ (100) | 41.1 | |
| $\alpha$ (111) | 43.8 | 44 |
| $\varepsilon$ (101) | 46.9 | |
| $\alpha$ (200) | 51 | 51.2 |
| $\alpha$ (220)/$\varepsilon$ (110) | 75.1 | 75.3 |

$\alpha$ = fcc phase, $\varepsilon$ = hcp phase.

*2.4. Tribological Measurements: Pin-On-Disk Tribometry and Dynamic Light Scattering*

The tribological properties of the sliding contacts of CoCrMo pin/UHMWPE disc with or without surface modification of CoCrMo pins were characterized by means of pin-on-disk tribometry (CMS Instruments SA, Peseux, Switzerland). Foetal bovine serum (FBS) was employed as the model synovial fluid [40,41]. The applied load, sliding speed and total sliding distance were 10 N, 50 mm/s and 1000 m, respectively. The coefficient of friction, $\mu$, defined as $\mu$ = friction/load, was recorded over the entire sliding contacts with the pin-on-disk tribometer. Wear properties of tribopair samples were characterized by means of the gravimetric method, optical inspection (photographs) of FBS containing wear debris and the hydrodynamic size ($D_H$) distribution of wear debris in FBS with dynamic light scattering (DLS). A Zetasizer (DLS, Zetasizer ZSP model, Malvern Instruments Ltd., Worcestershire, UK) was employed for DLS measurements. To this end, FBS containing wear particles was re-collected using a micropipette. Disposable cuvettes (PMMA, Brand™, Wertheim, Germany) were used for DLS measurements.

*2.5. Surface Roughness Measurements*

The 2D surface profile and the amplitude roughness parameters, namely (a) the arithmetic mean deviation (Ra) and (b) maximum height (Rz), were measured using a portable roughness gauge (Rugosurf 10G, TESA Technology, Telford, Shropshire, UK). The surface profile and parameters were measured in accordance with the Standard ISO4287/JIS B0601. The cut-off length was 2.5 mm. A total of 12 measurements was taken at different locations at the laser-treated surface. The average with standard deviation of $n$ = 12 was used to represent the Ra and Rz of the surface. The measurements were made in both directions including parallel and perpendicular to the laser tracks at the top surface of the laser-treated sample. Because no statistically-significant difference can be identified from the two datasets, only the results of one dataset (i.e., parallel to the laser tracks) were reported here.

*2.6. Vickers Microhardness Tests*

The hardness of the cross-section surface was measured by a Vickers microhardness testing machine under a constant load of 200 kgf. Three indentation marks were made in different locations down from the laser-formed surface coating to the base metal. Indentation Mark 1 was measured at 15 μm below the laser-formed coating, and indentation Marks 2 and 3 were measured at 65 and 115 μm below the coating, respectively. The distance between each indentation mark was 50 μm. At least three measurements were taken for each location to ensure the repeatability of the data, and the reported result was the average of the multiple measurements.

## 3. Results and Discussion

*3.1. Surface Morphology Analysis*

Figure 1 shows the optical micrograph images of the laser-treated pin and disc at different magnifications of 20× and 40×. Distinctive laser-melted tracks can be observed from the image in Figure 1. The laser tracks were about 200 μm in width with circular-ripple features inside the tracks. The direction (upward/downward) of the ripple features indicated the moving path of the laser beam in the laser remelting experiment. Temmler et al. [29,30] proposed a schematic model to explain that the resulting surface topography (i.e., surface ripples) in laser remelting is controlled by the variation of the melt pool volume and the movement of the three-phase line, namely the boundary between liquid and solid material and atmosphere, in the area of the solidification front. The ripple formation results from the fluctuation of the melt pool volume, which can be precisely modulated by the modulation of laser power. In other words, the surface topography can be controlled and optimised with a proper selection of laser power. Optical micrograph images of UHWMPE were flat and featureless except for occasional grinding marks. Representative images are shown in Figure S1 in the Supplementary Materials.

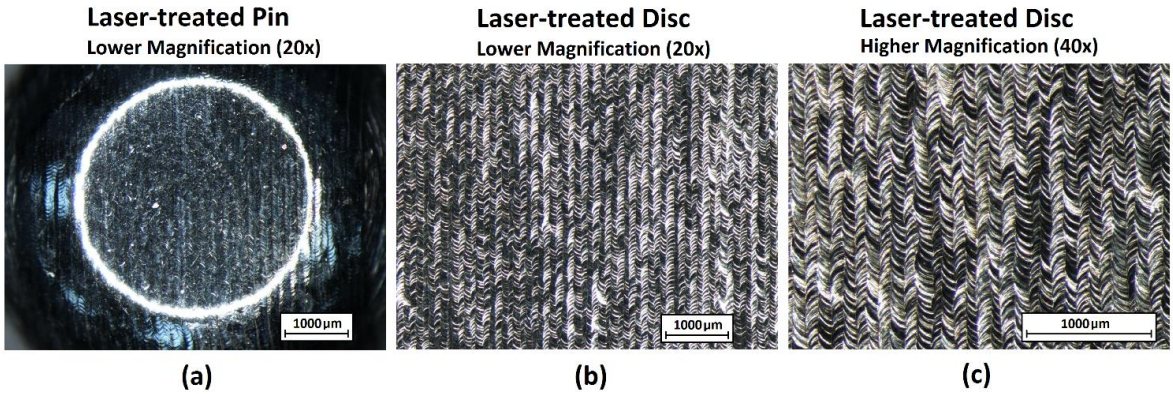


**Figure 1.** Optical micrograph image of laser-treated (**a**) pin (20× magnification), (**b**) disc (20× magnification) and (**c**) disc (40× magnification).

*3.2. Frictional Properties*

Throughout this study, one friction measurement was carried out per tribopair. Thus, statistical information on the friction forces is missing in this study. First, the frictional properties of the self-mated CoCrMo surfaces, with or without laser remelting, as characterized by pin-on-disc tribometry, are presented in Figure 2.

For both cases, after a somewhat chaotic run-in period, the $\mu$ values started to be stabilized with a slightly increasing trend until the end of measurements. The average and final $\mu$ values for the CoCrMo/CoCrMo pair were 0.239 ± 0.022 and 0.274, respectively, and those for the CoCrMo*/CoCrMo* pair were 0.163 ± 0.010 and 0.172, respectively. The $\mu$ values from the CoCrMo*/CoCrMo* pair were clearly lower than those of the CoCrMo/CoCrMo pair over the entire

duration of experiments. This result showed that laser remelting had a beneficial effect on the tribological properties of self-mated sliding contacts of CoCrMo surfaces.

The $\mu$ values obtained when one surface of self-mated sliding contacts of CoCrMo or CoCrMo* was replaced with a UHMWPE surface, either as pin or disc, under the same conditions are presented in Figure 3.

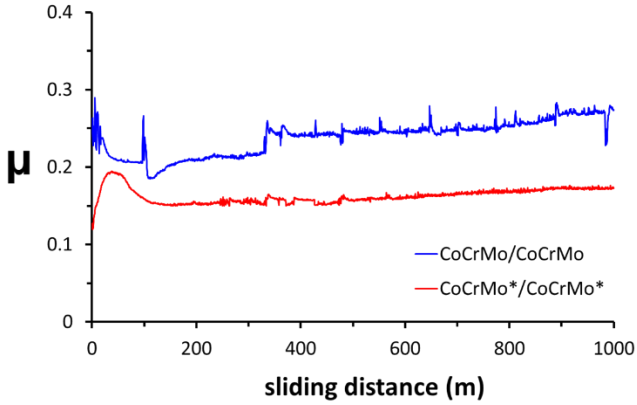


**Figure 2.** The variation of $\mu$ values for the CoCrMo/CoCrMo and CoCrMo*/CoCrMo* tribopairs with or without laser remelting (load = 10 N, sliding speed = 50 mm/s, lubricant: FBS).

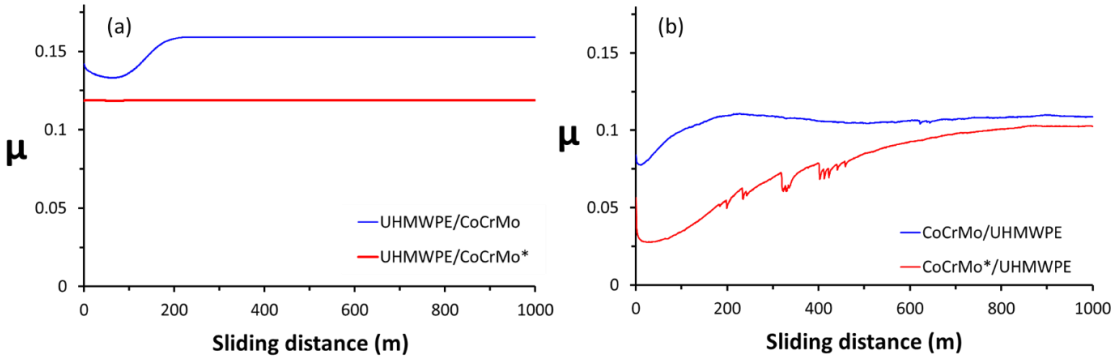


**Figure 3.** The $\mu$ vs. distance for (**a**) ultrahigh molecular weight polyethylene (UHMWPE)/CoCrMo and UHMWPE/CoCrMo* (**b**) CoCrMo/UHMWPE and CoCrMo*/UHMWPE in FBS. The load was 10 N, and the sliding speed was 50 mm/s.

The $\mu$ values were observed to be comparable to or smaller than those of corresponding CoCrMo/CoCrMo or CoCrMo*/CoCrMo* pairs. A few characteristics are noticed. Firstly, for both combinations of CoCrMo and UHMWPE surfaces, laser remelting of CoCrMo led to the reduction in the $\mu$ values of the tribopairs. This pair represents one of the most widely used and 'slippery' bearing pairs that are clinically used as orthopaedic implants [2,3,6], and this observation demonstrates that laser remelting of CoCrMo can improve the tribological properties even when the counter-surface is UHMWPE. Secondly, the UHMWPE/CoCrMo pair displayed higher $\mu$ values compared to its inverse configuration, i.e., CoCrMo/UHMWPE, even though the two tribopairs are composed of identical materials. Different tribological properties of unsymmetrical tribopairs in opposite configurations (i.e., A sliding on B vs. B sliding on A) are often reported [42], and it is generally ascribed to inequivalent energy dissipation in the two processes. In the present case, however, the larger diameter of the UHMWPE pin than the CoCrMo pin (see Section 2.1 above) and the consequent larger contact area appear to be the dominant reasons for higher friction forces and $\mu$ values. Related to this issue, the $\mu$ values for the UHMWPE/CoCrMo pair was fairly constant over the entire sliding duration, whereas a significant variation (overall, a gradual increase) was observed from the CoCrMo/UHMWPE pair, especially after laser remelting. Since the $\mu$ values of CoCrMo*/UHMWPE gradually increased from ca. 0.03 in the beginning to ca. 0.1 at the end of experiments, we can relate

this behaviour to a significant change of the CoCrMo*/UHMWPE interface, e.g., polishing effect, during the sliding contacts.

*3.3. Wear Properties*

The wear properties of the tribopairs were firstly characterized by means of the gravimetric method. The masses of the pin or disk for each tribopair before and after the test, as well as the changes in the mass are presented in Figure 4. Red and blue bars represent net loss and gain in mass, respectively.

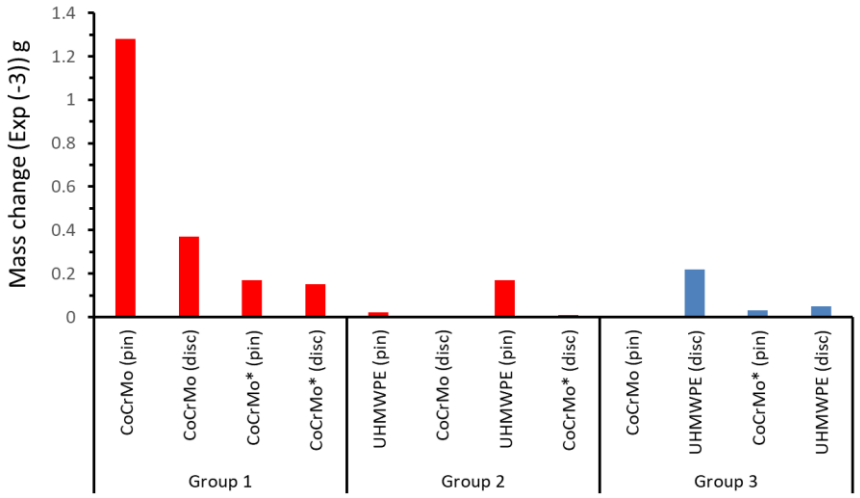


**Figure 4.** Mass changes in bearing materials after the tribological tests shown in Figures 2 and 3. Blue bars represent gains in the mass, and red bars represent losses in the mass.

A few characteristic behaviours were observed. Firstly, a beneficial tribological effect of laser remelting on the CoCrMo/CoCrMo pair was clearly observed in the wear properties, as well. Secondly, unlike the other tribopairs, CoCrMo/UHWMPE and CoCrMo*/UHWMPE pairs showed a net gain in mass changes as represented by blue bars. A net gain in mass after tribological tests including UHMWPE or other polymeric materials in simulated synovial fluids has often been reported in the literature [43,44], and it was attributed to absorption of fluid (FBS in this study) into the network of polymeric bearing materials. As net mass gain was not observed from the opposite configuration i.e., UHMWPE/CoCrMo or UHMWPE/CoCrMo*, we propose that the portion of UHMWPE disc surface that is free from tribological stress is mainly responsible for the absorption of fluids. In turn, this observation implies that the validity of the determination of wear properties by the gravimetric method is significantly weakened for polymeric materials. Thirdly, for the UHMWPE/CoCrMo pair, the mass loss was coming exclusively from UHMWPE, rather than CoCrMo. This is readily expected as the hardness of CoCrMo is substantially higher than UHMWPE. Lastly, for the UHMWPE/CoCrMo pair, the mass loss is greater after CoCrMo was laser treated. This is probably because the laser-treated CoCrMo surface is rougher and harder than untreated CoCrMo surfaces, as will be discussed below. Given that the friction forces of the UHMWPE/CoCrMo pair were reduced after laser remelting (Figure 2), the lower friction forces of this pair are accompanied by higher wear properties. It can thus be suggested that higher wear from the sliding of the UHMWPE pin on the laser-treated CoCrMo surface may lead to the transfer of UHMWPE, effectively reducing the interfacial shear strength between them.

The wear properties of the tribopairs were assessed by means of optical inspection and DLS of FBS re-collected after tribological tests, as well. Figure 5 shows the photographic pictures of FBS before and after the tribological experiments.

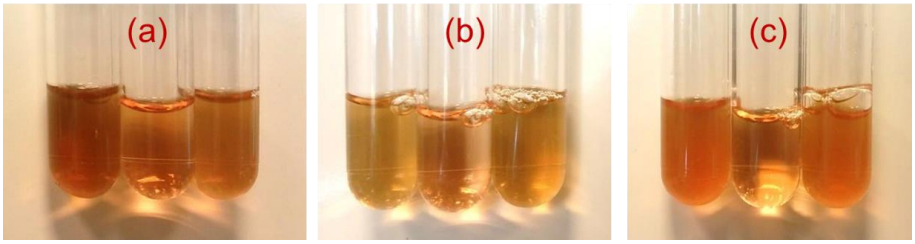


**Figure 5.** Colour changes in FBS: (**a**–**c**) corresponding to Groups 1, 2 and 3 in the mass changes in Figure 4 (i.e., (**a**) = Group 1, (**b**) = Group 2 and (**c**) = Group 3). In each group, the middle one is pristine FBS (no wear particles), and the samples on the left and right correspond to without (left) and with (right) laser remelting.

In general, the colour changes of FBS after tribological tests were not significant, and this is in a strong contrast with a previous study where self-mated titanium-based materials were employed as the tribopair [28]. In that study, unmodified titanium-based materials, e.g., Cp Ti Gr 2 or TiAlV alloys, led to a serious blackening of FBS caused by wear debris. Much less pronounced changes in the colours of FBS in this study supports that CoCrMo/UHMWPE is indeed a highly wear-resistant tribopair as bearing materials for artificial joints [2,3]. Nevertheless, it is also noticeable that FBS for CoCrMo/CoCrMo in Figure 5a is apparently darker than pristine FBS or that for the CoCrMo*/CoCrMo* pair. This is consistent with lower friction forces (Figure 2) and lower gravimetric wear (Figure 4) observed from the CoCrMo*/CoCrMo* tribopair, rather than its un-treated counterpart, and further supports the beneficial effect of laser remelting on the tribological properties. For UHMWPE/CoCrMo and UHMWPE/CoCrMo* pairs (Figure 5b), the mass loss is relatively smaller than from the other pairs (see Figure 4) such that the change of colour of FBS is ignorable. Moreover, FBS for CoCrMo/UHMWPE and CoCrMo*/UHMWPE appear to be slightly darker than pristine FBS, which suggests that a sizeable amount of wear debris may have been generated, although it was not possible to identify it by the gravimetric method (Figure 4).

Hydrodynamic size distribution, $D_H$ and Z-average values of wear particles in FBS of all the tribopairs are displayed in Figure 6.

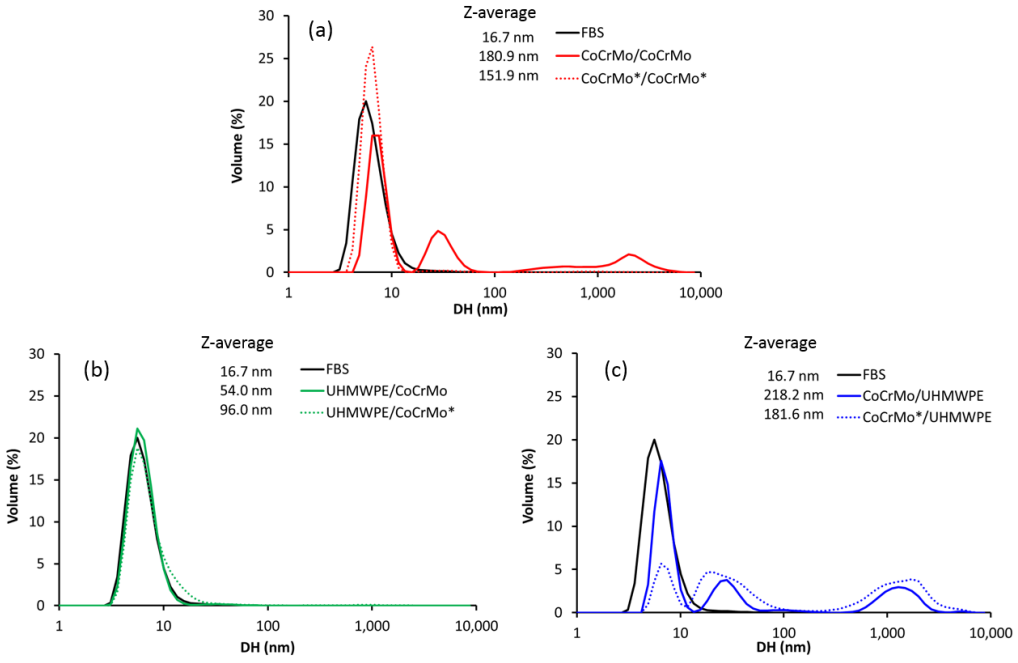


**Figure 6.** Distribution of hydrodynamic dimeter ($D_H$) and Z-average values of FBS before and after tribological experiments with various tribopairs: (**a**) CoCrMo/CoCrMo and CoCrMo*/CoCrMo* pairs, (**b**) UHMWPE/CoCrMo and UHMWPE/CoCrMo* pairs and (**c**) CoCrMo/UHMWPE and CoCrMo*/UHMWPE pairs.

Pristine FBS was employed as a reference from which a single peak with a maximum at ca. 7 nm and Z-average of 16.7 nm were observed. The $D_H$ distribution of FBS for CoCrMo/CoCrMo pairs (Figure 6a) showed the favourable effect of laser remelting in the wear-resistant properties of CoCrMo by showing that the peaks for large $D_H$, including the peak at ca. 50 nm and another broad peak from 200–5000 nm, disappeared after laser remelting. In addition, Z-average value was reduced by ca. 16% (from 180.9 nm–151.9 nm). However, it should be also noted that compared to pristine FBS, the Z-average increased enormously, namely to ca. 983% and 809% for CoCrMo/CoCrMo and CoCrMo*/CoCrMo*, respectively. This is consistent with more turbid colours of FBS after the tribological tests (Figure 5a). For UHMWPE/CoCrMo pairs (Figure 6b), the increase of the Z-average after laser remelting is the largest (ca. 78%). In contrast, this pair presented the smallest increase of the Z-average compared to that of pristine FBS (to ca. 223% and 475% for UHMWPE/CoCrMo and UHMWPE/CoCrMo* pairs, respectively), and this is consistent with the least magnitude of colour change after the tribostress (Figure 5b). Moreover, the $D_H$ distribution of FBS for UHMWPE/CoCrMo* was nearly overlapped with those of UHMWPE/CoCrMo or pristine FBS, supporting the generation of the least wear debris from this pair. Lastly, for the case of FBS with the CoCrMo/UHMWPE pair (Figure 6c), the appearance of larger peaks in the distribution of $D_H$ compared to pristine FBS is clear. In addition, Z-average values were in the order of FBS (16.7 nm) < UHMWPE/CoCrMo* (181.6 nm) < UHMWPE/CoCrMo (218.2 nm), which supports the favourable tribological effect of laser remelting, as shown in Figure 3. Overall, DLS results were more sensible than gravimetric wear analysis, especially when UHMWPE was involved.

### *3.4. Surface Roughness Measurements*

The 2D surface profile of the laser-treated CoCrMo disc is measured and shown in Figure 7a. The surface profile of the untreated surface is provided in Figure 7b to indicate the change in surface texture caused by laser remelting.

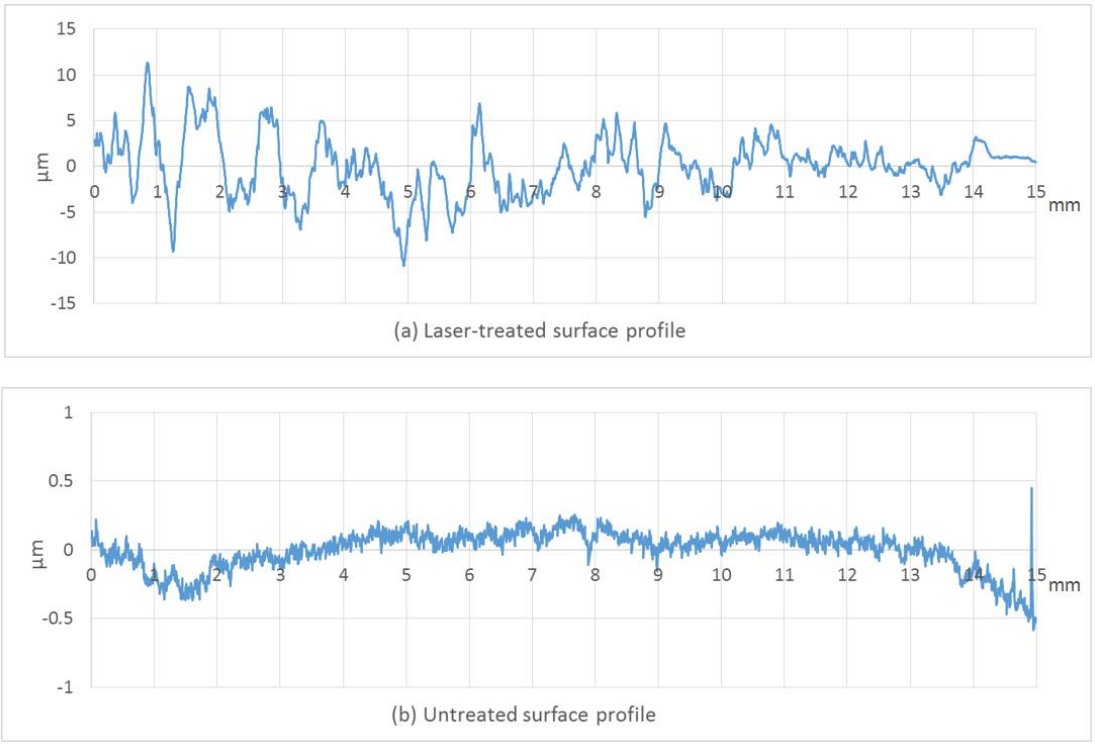


**Figure 7.** 2D surface profile of the (**a**) laser-treated and (**b**) untreated surfaces measured according to the Standard ISO 4287 (or JIS B0601). The surface profile result of the laser-treated surface is represented in the scale between ±15 µm whereas it is between ±1 µm for the untreated surface.

Regarding the surface profile, noticeable peaks and troughs can be identified from the laser-treated surface in Figure 7a. Comparing with the untreated surface (in Figure 7b), the peak-to-trough amplitude of the laser-treated surface was greater. To quantify the results, the surface roughness parameters, namely Ra (arithmetical mean deviation) and Rz (maximum height), are extracted from the surface profile and plotted in Figure 8a,b.

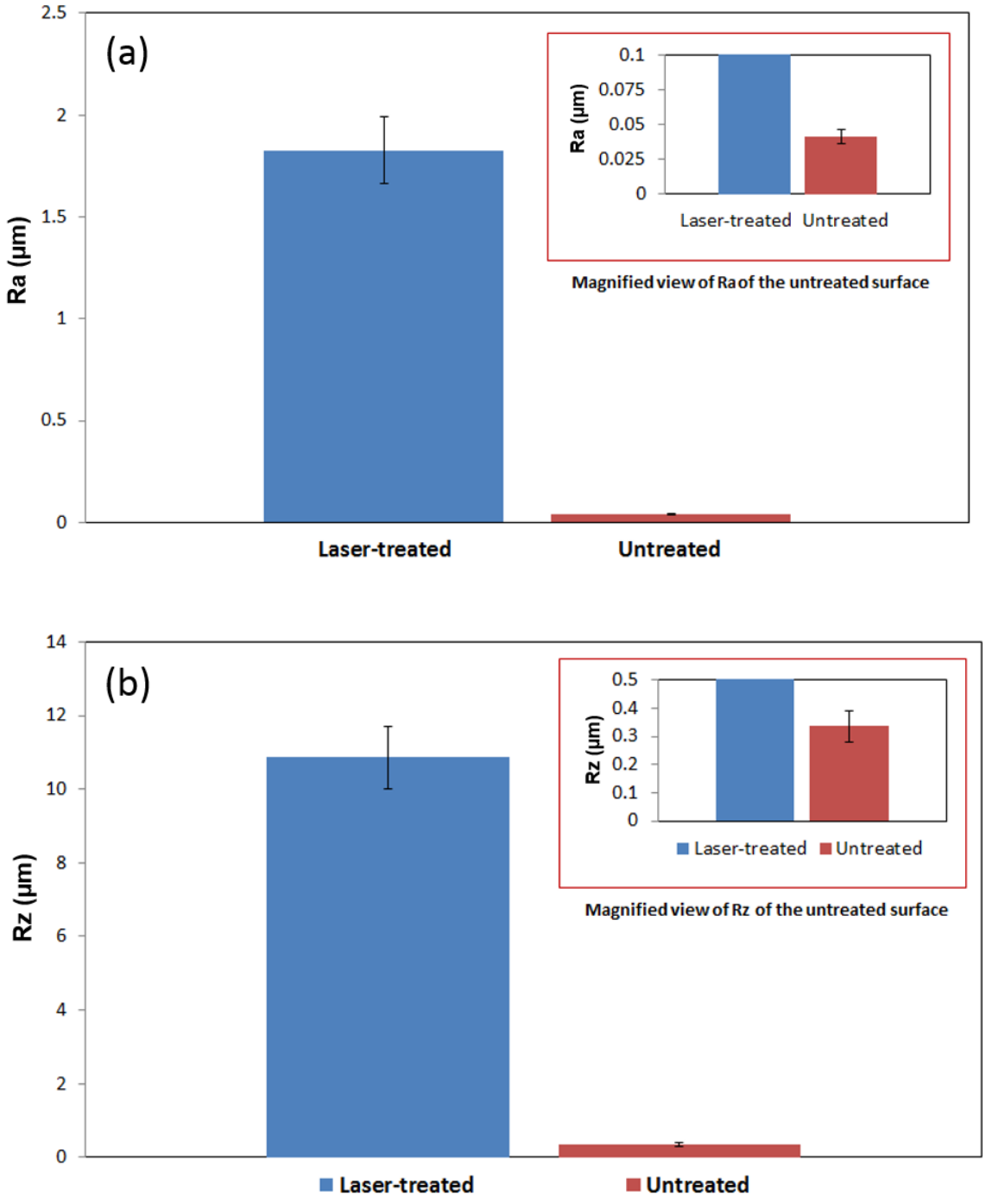


**Figure 8.** (**a**) Arithmetic mean deviation (Ra) and (**b**) maximum height (Rz) of the roughness profiles of the laser-treated and untreated CoCrMo surfaces (in Figure 7). The insets show the magnified view of Ra and Rz vs. of the untreated surface. The error bars indicated the standard deviation (SD) of $n = 12$.

The results in Figure 8 indicated that laser remelting significantly roughened the CoCrMo surface. Both the Ra and Rz values of the surface increased more than ten-fold after laser remelting. It is widely accepted that surface roughness played a significant role in determining the friction, as it directly controlled the actual contact area between the touching surfaces during sliding [45]. It should be noted that while laser remelting of the CoCrMo surface demonstrated a friction-reducing effect for all the tribopairs (Figure 2), wear properties displayed diverse effects depending on the tribopair (Figures 3–6). Thus, overall tribological effects of laser remelting of the CoCrMo surface cannot be simply accounted for by the increased Ra and Rz alone, which only describe the amplitude information of the surface profile after laser remelting.

*3.5. Vickers Microhardness Tests*

Hardness of metals/alloys has been long considered as one of the most important mechanical properties in wear and has been widely adopted as an indicator to determine the wear resistance [46]. In order to understand the effect of laser remelting on the wear behaviour of the CoCrMo alloy, the hardness of the laser-treated surface was measured. The micrograph in Figure 9 shows the existence of a laser-formed coating and the three indentation marks left in the cross-section surface after the hardness test. It can be observed in Figure 9 that Indentation Mark 1 had an unsymmetrical shape with the upper half area smaller than the lower half, whilst Indentation Marks 2 and 3 exhibited a typical symmetrical diamond shape.

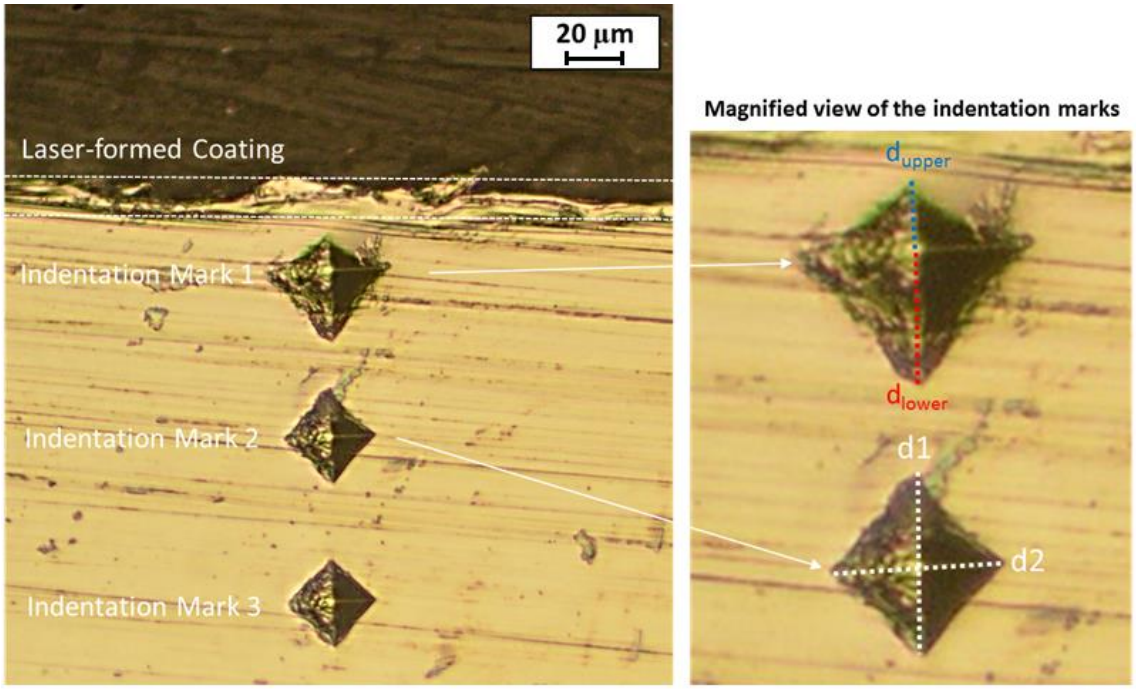


**Figure 9.** Optical micrograph image of the indentation marks left in the laser-treated CoCrMo at different locations.

In the Vickers microhardness test, the hardness of a material is determined by measuring the length of the diagonal of the indentation mark. The shorter the diagonal, the higher the hardness of the material. Usually, the average length of the two diagonals is used to calculate the Vickers hardness. The Vickers hardness is calculated using the equation below:

$$HV = 1.854\ F/d^2,$$

where $F$ is the applied load (kilogram-force or kgf) and $d$ is the average length of the two diagonals (mm).

After calculation, the hardness of the areas Indentation Marks 2 and 3 is determined as 391 and 412 HV, respectively. Given the unsymmetrical shape of Indentation Mark 1, the hardness cannot be

straightforwardly determined using the above equation. Nevertheless, the hardness of the upper and lower half areas of Indentation Mark 1 can still be analysed qualitatively by comparing the diagonal of the two areas, namely $d_{upper}$ and $d_{lower}$ (refer to Figure 9), with the half of the average diagonal of Indentation Marks 2 and 3. These values are given in Table 2.

**Table 2.** The length of diagonals measured from the indentation marks in Figure 9.

| **Indentation Mark 1** | | **Indentation Mark 2** | **Indentation Mark 3** |
|---|---|---|---|
| Diagonal of the upper half area, $d_{upper}$ (μm) | Diagonal of the lower half area, $d_{lower}$ (μm) | Half of the average diagonal $(d1 + d2)/4$ (μm) | |
| 12.6 | 22.4 | 15.4 | 15.0 |

If the $d_{upper}$ (or $d_{lower}$) is smaller than the half of the average diagonal of Indentation Marks 2 and 3, it gives an indication that the upper (or lower) half area of Indentation Mark 1 is harder than the area in Indentation Marks 2 and 3. By using this relationship, it is known that the upper half area is harder, whilst the lower half area is softer when compared to the hardness of areas in Indentation Marks 2 and 3. The unsymmetrical shape of Indentation Mark 1 also indicated that the hardness of the area right below the laser-formed coating (i.e., within the depth of 15 μm) increased while the hardness decreased in the depth between 15 and 35 μm below the coating. The nearly identical size of Indentation Marks 2 and 3 indicated that there is only a little change in hardness after the depth of 50 μm below the coating, which can be evidenced by their similar values of hardness.

The findings pointed to the fact that laser remelting created a coating in the surface and a laser-affected zone underneath the coating. The laser-affected zone can be sub-divided into the hardened zone and the softened zone. The thickness of the hardened zone was measured as approximately 20 μm. Figure 10 shows the graphical representation of the laser-treated surface for the CoCrMo alloy. The impact of the hierarchically-generated hardened zone and softened zone on the tribological properties of CoCrMo is presently unclear. More importantly, the hardness of the laser-formed coating, which is expected to play a bigger role in determining the tribological properties, could not be determined by the current method as the size of indenter was larger than the coating thickness.

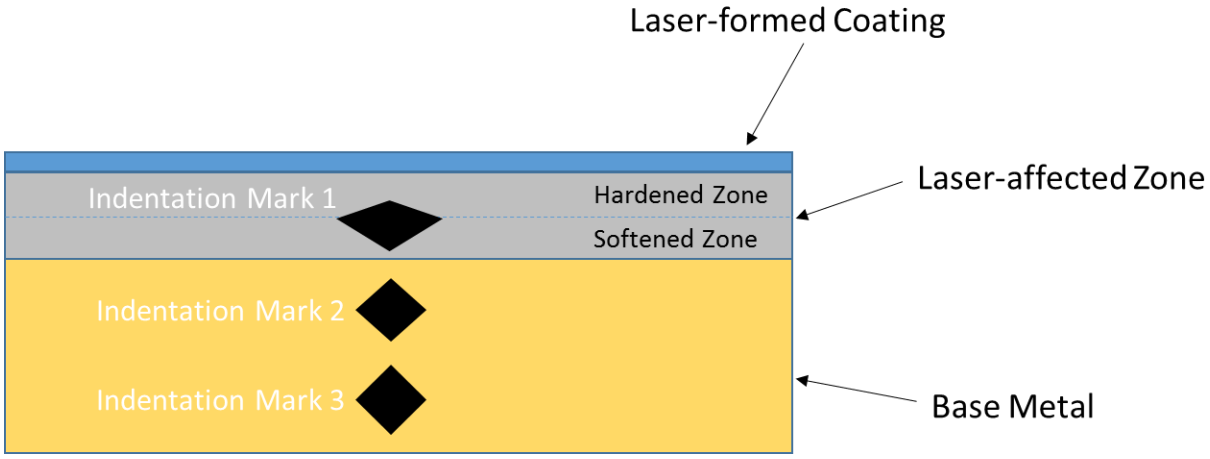


**Figure 10.** Graphical representation of the cross-section structure of the laser-treated CoCrMo surface. The laser-treated surface was composed of three different zones, namely laser-formed coating at the top, laser-affected zone in the middle, followed by the base metal at the bottom. The laser-affected zone can be sub-divided into the hardened zone (upper) and softened zone (lower).

*3.6. Surface Phase Structure Analysis*

Figure 11 shows the XRD profile for the laser-treated and untreated surfaces. It is important to point out that the penetration depth of the radiation into the material surface is typically a few μm in

the XRD measurement [27]. The penetration depth is between 0.8 and 1.9 μm in our XRD (refer to Section 2.3). The thickness of the laser-formed coating varied between 5 and 15 μm (refer to Figure 9). It indicated that the XRD profile of the laser-treated surface reflected the phase structure of the laser-formed coating since the X-ray radiation cannot reach the laser-affected zone underneath the coating.

The XRD profile of the untreated CoCrMo surface (in Figure 11) showed the co-existence of the $\alpha$ phase and $\varepsilon$ phase. The $\alpha$ phase is face-centred cubic (fcc), which is metastable (i.e., only stable at high temperature), whilst the $\varepsilon$ phase has the hexagonal close-packed structure (hcp) and is stable at ambient temperature. The phase peaks of (111) at 43.8°, (200) at 51° and (220) at 75.1° indicated the presence of the fcc $\alpha$ phase in the untreated surface, whilst the presence of the hcp $\varepsilon$ phase is evidenced by the peaks of (100) at 41.1° and (101) at 46.9°. In comparison, the laser-formed coating showed only the $\alpha$ phase peaks of (111) at 44°, (200) at 51.2° and (220) at 75.3°, with slight shifts to a higher angle. It is believed that the $\alpha$ phase formed as non-equilibrium phase during the rapid cooling in the laser remelting process and that the angle shifts are due to the lattice compression after laser remelting. The laser-formed coating exhibited a more homogeneous phase structure than the untreated surface (or base metal).

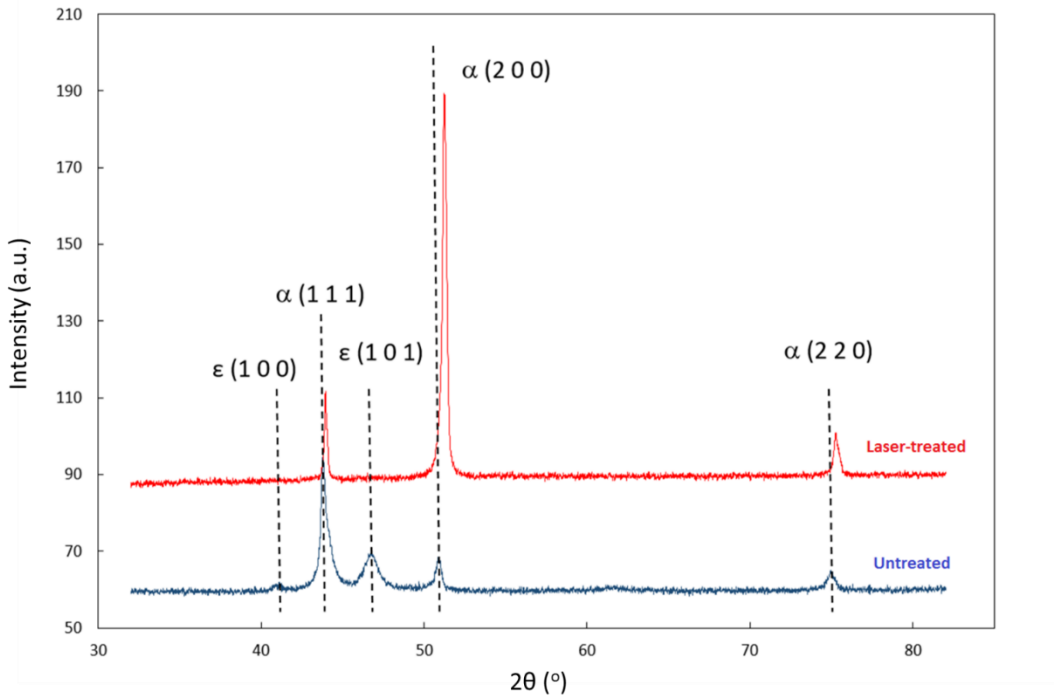


**Figure 11.** XRD profile for the laser-treated and untreated surfaces.

There is no evidence for the formation of any nitride phases in these data. The detection limit in XRD under the conditions used is estimated at <0.2%. Adapting the method of Cullity [37] suggests that 0.2% of the signal from the CoCrMo material would originate from the outermost 5 nm only, placing a maximum upper limit around this value on the thickness of any nitride layers present.

Although the hardness of the laser-formed layer cannot be directly measured in the Vickers hardness test as mentioned above, the homogenous phase structure can contribute to increasing the hardness, which may account for the reduced friction and wear properties from the CoCrMo/CoCrMo interface after laser remelting (Figures 2 and 4–6), as well as increased wear properties of the UHMWPE/CoCrMo interface (Figures 4 and 6) after laser remelting. Increased hardness of CoCrMo due to the laser-induced fine and homogenous microstructure has been reported by a number of authors [18,19,23,24]. Since no nitride was detected in XRD, the possibility of hardness increment due to the nitride formation can be ruled out.

On the other hand, it is known that a small amount of carbon is incorporated into the CoCrMo alloy as carbides, namely $M_{23}C_6$ and $M_6C$ (i.e., M = Cr, Mo, Co), during the casting process. These carbides can significantly influence the mechanical properties of CoCrMo. It is generally accepted that the size and location of the carbides in the grains can have different impacts on the strength of CoCrMo alloy. Fine carbide precipitates within the grains can increase the strength, whereas coarse carbides at grain boundaries can embrittle the material. Further, the findings of Liao et al. indicated that the homogeneity of the carbides in CoCrMo is dependent on the cooling rate in the solidification process, with the higher cooling rate favouring the formation of more homogeneous and harder carbides [47]. The CoCrMo alloy underwent rapid cycles of melting and solidification processes during the laser remelting. The cooling rate in laser remelting can reach to $10^5$ °C/s, significantly higher than in conventional processes (i.e., 0.2–50 °C/s). It is believed that the increased hardness in the hardened zone (i.e., situated right below the laser-formed coating) can be related to the precipitation of homogeneous carbides induced by the rapid cooling rate in the laser remelting. Likewise, the presence of the softened zone can be associated with carbide precipitation and the aforementioned carbide-related parameters, such as their size, location and homogeneity. However, it is inconclusive to determine the mechanisms of how these carbide precipitates affected the mechanical properties of the laser-affected zones and more importantly how they can lead to the formation of hardened and softened zones. A more focused and in-depth microstructural study (i.e., TEM) will be required to provide insight into the relationship between the carbide precipitation and laser remelting processes.

Overall, we propose that the reduced $\mu$ values (Figure 2) and wear (Figures 4–6) for the self-mated sliding contacts of CoCrMo after laser remelting result chiefly from an increase in hardness of the top-most layer (i.e., laser-formed coating). On the other hand, reduced $\mu$ values for CoCrMo/UHMWPE or UHMWPE/CoCrMo pairs (Figure 2b,c), yet increased wear for the UHMWPE/CoCrMo pair (Figure 4) after laser remelting, can be explained by increased transfer of polymeric material to the metallic side, caused by the increased surface roughness and hardness of the laser-formed coating.

## 4. Conclusions

Even though CoCrMo/CoCrMo and CoCrMo/UHMWPE tribopairs are highly popular as bearing materials for arthroplasty thanks to their reliable tribological performance and excellent biocompatibility, the generation of wear debris and consequently limited service time is an unsolved problem to date. In this preliminary study, we have demonstrated that laser remelting of the CoCrMo surface can lead to improved friction and wear-resistant properties of both tribopairs. The important results arising from this study can be summarised as follows:

(i). The laser-formed coating exhibited a homogeneous phase structure. The coating showed only the $\alpha$ phase peaks (i.e., no $\varepsilon$ phase detected).
(ii). Laser remelting of the CoCrMo surface demonstrated a friction-reducing effect for all the tribopairs (namely, (a) CoCrMo pin-on-CoCrMo disc, (b) UHMWPE pin-on-CoCrMo disc and (c) CoCrMo pin-on-UHMWPE disc).

**Supplementary Materials:** The following are available online at www.mdpi.com/link: Figure S1: Optical microscopic images of UHWMPE pin (left) and disc (right) before tribological tests. The scale bars represent 1 mm.

**Acknowledgment:** The laser remelting work described in this paper was supported by a research grant from the School of Mechanical and Aerospace Engineering, Queen's University, Belfast (Research Fund: D8201MAS), United Kingdom.

**Author Contributions:** CWC conceived, designed and performed the laser remelting experiments; SL conceived, designed and performed the tribological tests. GCS contributed to perform and analyse the XRD measurements. CWC, SL and GCS contributed equally to write this paper.

**Conflicts of Interest:** The authors declare no conflict of interest.

## References


1. Health at a Glance: Europe 2016, State of Health in the EU Cycle, OECD. Available online: http://dx.doi.org/10.1787/9789264265592-en (accessed on 25th January 2018).
2. Kurtz, S.M. *The UHMWPE Handbook: Ultra-High Molecular Weight Polyethylene in Total Joint Replacement*; Springer: New York, NY, USA, 2009.
3. Knahr, K. *Tribology in Total Hip Arthroplasty*; Springer: New York, NY, USA, 2011.
4. Learmonth, I.D. Biocompatibility: A biomechanical and biological concept in total hip replacement. *Surg. J. R. Coll. Surg. Edinb. Irel.* **2003**, *1*, 1–8.
5. Ingham, E.; Fisher, J. The role of macrophages in osteolysis of total joint replacement. *Biomaterials* **2005**, *26*, 1271–1286.
6. Buford, A.; Goswami, T. Review of wear mechanisms in hip implants: Paper I—General. *Mater. Des.* **2004**, *25*, 385–393.
7. Buford, A.; Goswami, T. Review of wear mechanisms in hip implants: Paper II—Ceramics IG004712. *Mater. Des.* **2004**, *25*, 395–405.
8. Ingham, E.; Fisher, J. Biological reactions to wear debris in total joint replacement. *Proc. Inst. Mech. Eng. H* **2000**, *214*, 21–37.
9. Liu, R.; Li, X.; Hu, X.; Dong, H. Surface modification of a medical grade Co.-Cr-Mo alloy by low-temperature plasma surface alloying with nitrogen and carbon. *Surf. Coat. Technol.* **2013**, *232*, 906–911.
10. Wang, Q.; Zhang, L.; Dong, J. Effects of plasma nitriding on microstructure and tribological properties of CoCrMo alloy implant materials. *J. Bionic Eng.* **2010**, *7*, 337–344.
11. Walker, J.C.; Cook, R.B.; Murray, J.W.; Clare, A.T. Pulsed electron beam surface melting of CoCrMo alloy for biomedical applications. *Wear* **2013**, *301*, 250–256.
12. Galetz, M.C.; Fleischmann, E.W.; Konrad, C.H.; Schuetz, A.; Glatzel, U. Abrasion resistance of oxidized zirconium in comparison with CoCrMo and titanium nitride coatings for artificial knee joints. *J. Biomed. Mater. Res. B Appl. Biomater.* **2010**, *93*, 244–251.
13. Galetz, M.C.; Seiferth, S.H.; Theile, B.; Glatzel, U. Potential for adhesive wear in friction couples of UHMWPE running against oxidized zirconium, titanium nitride coatings, and cobalt-chromium alloys. *J. Biomed. Mater. Res. B Appl. Biomater.* **2010**, *93*, 468–475.
14. Van Hove, R.P.; Sierevelt, I.N.; van Royen, B.J.; Nolte, P.A. Titanium-nitride coating of orthopaedic implants: A review of the literature. *Biomed. Res. Int.* **2015**, *2015*, 485975.
15. Santos, C.B.; Haubold, L.; Holeczek, H.; Becker, M.; Metzner, M. Wear–corrosion resistance of DLC/CoCrMo system for medical implants with different surface finishing. *Tribol. Lett.* **2010**, *37*, 251–259.
16. Zhang, T.F.; Deng, Q.Y.; Liu, B.; Wu, B.J.; Jing, F.J.; Leng, Y.X.; Huang, N. Wear and corrosion properties of diamond like carbon (DLC) coating on stainless steel, CoCrMo and $Ti_6Al_4V$ substrates. *Surf. Coat. Technol.* **2015**, *273*, 12–19.
17. Corona-Gomez, J.; Shiri, S.; Mommadtaheri, M.; Yang, Q. Adhesion enhancement of DLC on CoCrMo alloy by diamond and nitrogen incorporation for wear resistant applications. *Surf. Coat. Technol.* **2017**, *332*, 120–127.
18. Meacock, C.G.; Vilar, R. Structure and properties of a biomedical Co–Cr–Mo alloy produced by laser powder microdeposition. *J. Laser Appl.* **2009**, *21*, 88–95, doi:10.2351/1.3120214.
19. Chen, C.J.; Xu, X.; Cao, Q.; Zhang, M.; Chang, Q.; Zhang, S. Laser surface cladding of plastic-molded steel 718H by CoCrMo alloy. *J. Mater. Eng. Perform.* **2012**, *21*, 946–950.
20. Barekat, M.; Razavi, R.S.; Ghasemi, A. Nd:YAG laser cladding of Co–Cr–Mo alloy on γ-TiAl substrate. *Opt. Laser Technol.* **2016**, *80*, 145–152.
21. Barekat, M.; Razavi, R.S.; Ghasemi, A. High temperature oxidation behavior of laser clad Co–Cr–Mo coating on γ-TiAl substrate. *J. Laser Appl.* **2016**, *28*, doi:10.2351/1.4958971.
22. Barekat, M.; Razavi, R.S.; Ghasemi, A. Wear behavior of laser-cladded Co–Cr–Mo coating on γ-tial substrate. *J. Mater. Eng. Perform.* **2017**, *26*, 3226–3238.
23. Monroy, K.P.; Delgado, J.; Sereno, L.; Ciurana, J.; Hendrichs, N.J. Effects of the selective laser melting manufacturing process on the properties of CoCrMo single tracks. *Met. Mater. Int.* **2014**, *20*, 873–884.
24. Mantrala, K.M.; Das, M.; Balla, V.K.; Rao, C.S.; Rao, V.V.S. Laser-deposited CoCrMo alloy: Microstructure, wear, and electrochemical properties. *J. Mater. Res.* **2014**, *29*, 2021–2027.

25. Mantrala, K.M.; Das, M.; Balla, V.K.; Rao, C.S.; Rao, V.V.S. Additive manufacturing of Co–Cr–Mo alloy: Influence of heat treatment on microstructure, tribological, and electrochemical properties. *Front. Mech. Eng.* **2015**, *1*, 1–7.
26. Sahasrabudhe, H.; Bose, S.; Bandyopadhyay, A. Laser processed calcium phosphate reinforced CoCrMo for load-bearing applications: Processing and wear induced damage evaluation. *Acta Biomater.* **2018**, *66*, 118–128.
27. Chan, C.W.; Lee, S.; Smith, G.C.; Sarri, G.; Ng, C.H.; Sharba, A.; Man, H.C. Enhancement of wear and corrosion resistance of beta titanium alloy by laser gas alloying with nitrogen. *Appl. Surf. Sci.* **2016**, *367*, 80–90.
28. Chan, C.W.; Lee, S.; Smith, G.C.; Donaghy, C. Fibre laser nitriding of titanium and its alloy in open atmosphere for orthopaedic implant applications: Investigations on surface quality, microstructure and tribological properties. *Surf. Coat. Technol.* **2017**, *309*, 628–640.
29. Temmler, A.; Willenborg, E.; Wissenbach, K. Design surfaces by laser remelting. *Phys. Procedia* **2011**, *12*, 419–430.
30. Temmler, A.; Schmickler, T.; Willenborg, E. Surface structuring by laser remelting of Inconcel 718. In Proceedings of the Lasers in Manufacturing Conference, Munich, Germany, 22–24 June 2015.
31. Yasa, E.; Kruth, J. Application of laser re-melting on selective laser melting parts. *Adv. Prod. Eng. Manag.* **2011**, *6*, 259–270.
32. Dong, C.; Gu, Y.; Zhong, M.; Li, L.; Ma, M.; Liu, W. The effect of laser remelting in the formation of tunable nanoporous Mn structures on mild steel substrates. *Appl. Surf. Sci.* **2011**, *257*, 2467–2473.
33. Guo, H.; Tian, Z.; Huang, Y.; Yang, H. Microstructure and tribological properties of laser-remelted Ni-based WC coatings obtained by plasma spraying. *J. Russ. Laser Res.* **2015**, *36*, 48–58.
34. Vaithilingam, J.; Goodridge, R.D.; Hague, R.J.M.; Christie, S.D.R.; Edmonds, S. The effect of laser remelting on the surface chemistry of $Ti_6Al_4V$ components fabricated by selective laser melting. *J. Mater. Process. Technol.* **2016**, *232*, 1–8.
35. Akinlabi, E.T.; Mahamood, R.M.; Akinlabi, S.A. *Advanced Manufacturing Techniques Using Laser Material Processing*; IGI Global: Hershey, PA, USA, 2016.
36. Chan, C.W.; Carson, L.; Smith, G.C.; Morelli, A.; Lee, S. Enhancing the antibacterial performance of orthopaedic implant materials by fibre laser surface engineering. *Appl. Surf. Sci.* **2017**, *404*, 67–81.
37. Cullity, B.D. *Elements of X-ray Diffraction*; Addison-Wesley Publishing Co. Inc.: Boston, MA, USA, 1978.
38. X-ray Mass Attenuation Coefficients. Available online: https://physics.nist.gov/PhysRefData/XrayMassCoef/tab3.html (accessed on 14th February 2018).
39. Guo, Z.; Pang, X.; Yan, Y.; Gao, K.; Volinsky, A.A.; Zhang, T.Y. CoCrMo alloy for orthopaedic implant application enhanced corrosion and tribocorrosion properties by nitrogen implantation. *Appl. Surf. Sci.* **2015**, *347*, 23–34.
40. Morillo, C.; Sawae, Y.; Murakami, T. Effect of bovine serum constituents on the surface of the tribological pair alumina/alumina nanocomposites for total hip replacement. *Tribol. Int.* **2010**, *43*, 1158–1162.
41. Bortel, E.L.; Charbonnier, B.; Heuberger, R. Development of a synthetic synovial fluid for tribological testing. *Lubricants* **2015**, *3*, 664–686.
42. Lee, S.; Heuberger, M.; Rousset, P.; Spencer, N.D. A tribological model for chocolate in the mouth: General implications for slurry-lubricated hard/soft sliding counterfaces. *Tribol. Lett.* **2004**, *16*, 239–249.
43. Afftato, S.; Vandelli, C.; Bordini, B.; Toni, A. Fluid absorption study in Ultra-high molecular weight polyethylene (UHMWPE) sterilized and unsterilized acetabular cups. *Proc. Inst. Mech. Eng. H* **2001**, *215*, 107–111.
44. Yao, J.Q.; Blanchet, T.A.; Murphy, D.J.; Laurent, M.P. Effect of fluid absorption on the wear resistance of UHMWPE orthopaedic bearing surfaces. *Wear* **2003**, *255*, 1113–1120.
45. Jiang, H.; Browning, R.; Fincher, J.; Gasbarro, A.; Jones, S.; Sue, H.J. Influence of surface roughness and contact load on friction coefficient and scratch behavior of thermoplastic olefins. *Appl. Surf. Sci.* **2008**, *254*, 4494–4499.
46. Jeong, H.; Erb, U.; Aust, K.T.; Palumbo, G. The relationship between hardness and abrasive wear resistance of electrodeposited nanocrystalline Ni–P coatings. *Scr. Mater.* **2003**, *48*, 1067–1072.
47. Liao, Y.; Pourzal, R.; Stemmer, P.; Wimmer, M.A.; Jacobs, J.J.; Fischer, A.; Marks, L.D. New insights into hard phases of cocrmo metal-on-metal hip replacements. *J. Mech. Behav. Biomed. Mater.* **2012**, *12*, 39–49.